The International Journal of Advanced Manufacturing Technology (2019) 104:2415–2427
https://doi.org/10.1007/s00170-019-03971-0

ORIGINAL ARTICLE

A study of wear on focusing tubes exposed to corundum-based abrasives in the waterjet cutting process

Andrzej Perec[1,2] · Frank Pude[1,3] · Anton Grigoryev[1] · Michael Kaufeld[3,4] · Konrad Wegener[1,5]

Received: 2 December 2018 / Accepted: 30 May 2019 / Published online: 6 July 2019
© Springer-Verlag London Ltd., part of Springer Nature 2019

Abstract

Corundum-based abrasives are commonly used for cutting extremely hard materials like e.g. ceramics by means of abrasive waterjets. Due to a reduced lifetime of the used focusing tubes, this type of abrasive is only applied under special consideration of economic circumstances. The cutting centres which use this technology retain only a small amount of used abrasives because of the limited application of this grain type. Nevertheless, observing the disintegration of particles which have interacted with mostly advanced materials is of scientific interest. Garnet-based abrasives are commonly classified in different grain size classes after sieving to evaluate their recycling potential. Based on a feasibility study, this paper will present some results on achieved cutting data and also shows the geometrical change of the used focusing tubes which was realized by non-destructive examination. The mass loss factor of the used focusing tubes was calculated for different corundum materials and compared with the commonly used in AWJ machining abrasive, garnet. Additionally, cutting and recycling properties of the tested corundum-based abrasive was tested. The disintegration properties of the corundum-based abrasive were monitored by sieving and optical test methods. Particle identification after cutting process (grain or chip) was realized by energy-dispersive X-ray microanalysis (EDX). Finally, the results obtained were used to make a rough calculation for lifetime estimations of the focusing tubes related to the observed wear process.

Keywords Abrasive · Waterjet · Corundum · Grain size · Disintegration

1 Introduction

Cutting by high-pressure waterjet is one of the high-tech methods of separating materials. Treating materials using a high-pressure abrasive waterjet is more complex than conventional treatments. High-pressure water is converted to a high-speed jet inside a nozzle (Fig. 1a) and flows out of the nozzle at a speed of several hundred meters per second, to entrain abrasive particles and accelerates them to large kinetic energies. Adding dry abrasives to the waterjet in a special mixing injector (Fig. 1b) increases cutting efficiency. As a result, it becomes possible to cut almost any material. For the Abrasive Water Injection Jet system (AWIJ), the most commonly used pressure ranges from 400 to 600 MPa.

This technology has many advantages: wide range of options, including the processing of complex shapes, the cutting of a large variety of materials, for example hybrid aluminium matrix composite, tested by Nag et al. [18], or bulk metallic glasses examined by Wessels et al. [32].

The big advantage is the environmental friendliness of this technology, noticed by both Kukielka [9] and Perec [23]. The high effectiveness and good quality of the surface, as observed by Perec [26] and Tavodova [29], is comparable to the quality which can be reached by forming processes, achieved by Kukielka et al. [8, 10] and Patyk et al. [20], or grinding, published by Kacalak [7] and Lipinski [13] from Koszalin University of Technology.

✉ Andrzej Perec
aperec@ajp.edu.pl

1 Inspire AG, ETH Zurich, Zurich, Switzerland

2 Department of Technology, Jacob of Paradies University, Gorzow Wlkp., Poland

3 Steinbeis Consulting Center High-Pressure Waterjet Technology, Horgau, Germany

4 Institute of Production Engineering and Materials Testing, University of Applied Sciences Ulm, Ulm, Germany

5 Institute of Machine Tools and Manufacturing (IWF), Swiss Federal Institute of Technology (ETH), Zurich, Switzerland

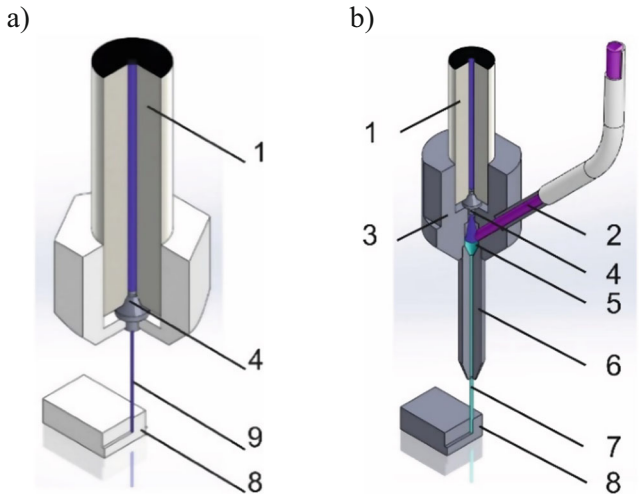

Fig. 1 Schematic diagram of **a** waterjet cutting and **b** abrasive water injection jet cutting: 1, high-pressure water inlet; 2, abrasive inlet; 3, cutting head body; 4, water nozzle, 5, mixing chamber; 6, focusing tube; 7, high-pressure abrasive waterjet; 8, machining sample; 9, high-pressure waterjet

Detailed studies of the surface quality machined by AWJ were the object of interest of various scientific teams. Valicek et al. [31] proposed an evaluation of the worst cut surface area based on the root mean square (RMS) roughness and the dimensionless statistical factor calculated as a basic quantity for AWJ surface cut characterization related also to the traverse speed of the cutting head. Lehocka et al. [2] compared the quality of a machined surface of graphite and aluminium alloy by abrasive waterjet under 400 MPa pressure with different water nozzle and focusing tubes. The change in focusing on tube diameter caused the change in values of roughness parameters. Krolczyk et al. [6] studied relations between the measured R_a, R_q, and R_z surface roughness parameters, the traverse speed, and the vibration parameters, generated during abrasive water jet cutting. Equations for prediction of the surface roughness parameters were derived according to the vibration parameter and the traverse speed. Spadło and Krajcarz [27] performed the surface studies of the evaluation of copper cutting surface, with special emphasis on the trajectory of the jet. They noticed of an effect of the reduction of the kinetic energy of the cutting jet along with material penetration the surface at the outlet of the jet from the machined material, a surface characterized by the occurrence of multi-directional traces of abrasive grains and confirmed the effect of embedding fragments of crushed grains on the surface of the processed material.

The most commonly used abrasive is garnet, which is shown, among others, by Sutowska et al. [28] and Perec [21]. It is popular in the processing stream because it achieves high performance, publicated by Galecki and Mazurkiewicz [5] at relatively low wear of the focusing tubes used [25]. The high flow rate jets research used quartz (silica) sand because of its low price [22].

Martin et al. [14] recommended a circumspect choice of the abrasive material which is to reach a compromise between nozzle lifetime and the machined material efficiency.

In practice, however, there is a need for industrial cutting of super hard materials like e.g. stellite, sintered tungsten carbide or even polycrystalline diamond (PCD). The use of garnet to cut such materials results in poor efficiency, or simply the inability to carry out processing.

Therefore, it seems to be expedient to conduct research on modern abrasives based e.g. on aluminium oxide—*corundum*. The results of preliminary research on the use of corundum for cutting low-alloy high-strength structural steel Q345 were published by Guan et al. [3]. As what they have observed during the AWJ cutting, there exists a pressure threshold, i.e. the jet pressure under which the abrasive erosion kinetic energy is just enough to induce material deformation.

2 Research materials

2.1 Corundum

Corundum is a very hard, tough, and stable mineral. It is the second hardest mineral after diamond. It is also unaffected by acids and most environments. Natural corundum occurs as contact metamorphic rocks (emery) and precious stones (sapphire, ruby). Translucent brown corundum and emery are the most common forms of corundum. These are fairly common and when ground up, they are the most favourable abrasives. The industrial term "emery" describing corundum abrasives is derived from the variety emery, which is mined for abrasive use [15]. The most important properties of corundum are shown in Table 1.

Artificial corundum (also fused alumina or artificial aluminium oxide) is a synthetic abrasive that consists mainly of crystallized alumina, or aluminium oxide, in the form (corundum) and also contains oxides of silicon, titanium, calcium, and iron [11, 30]. Artificial corundum is obtained by melting an alumina-containing raw material in an arc furnace and then allowing the melt to crystallize. Depending on the alumina content and the characteristics of the melting process, the following varieties of artificial corundum are distinguished: regular alumina, white alumina, modified alumina, single-crystal alumina, and spheroidal alumina. Regular alumina consists of up to 95% α-alumina and small amounts of slag and a ferroalloy as impurities. It is widely used to machine metals [12, 33].

Modified alumina may contain chromium oxide, titanium oxide, or zirconium oxide. Its properties depend on the composition and content of the impurities. Abrasive tools made from modified alumina are used to machine parts made of structural steel or certain tool steels. Abrasive tools made from single-crystal alumina are used to grind, for example heat-

Table 1 Properties of corundum [4, 15]

Chemical formula	Al_2O_3
Molar mass M	101.96 g/mol
Composition	Aluminium oxide
Hardness	9 (Mohs)
Microhardness	19–24 GT/m^2
Crystal system	Hexagonal
Crystal forms and aggregates	Crystals occur as hexagonally shaped prismatic and tabular crystals, and as bipyramid hexagons that are wider in the center and taper thinly on the ends. Crystals are usually elongated and striated crosswise, and sometimes occur in thin plates. Crystals are commonly smooth or rounded on the edges due to alluvial action. Also as barrel-shaped hexagonal crystals, modified octahedrons, massive, and as rounded, waterworn alluvial pebbles. Crystals are sometimes striated or etched.
Density	3900–4100 kg/m^3
Melting point TM	2015 °C
Boiling point TB	2980 °C
Lustre	Vitreous to adamantine

resistant or structural alloy steels or other alloys that are difficult to machine [16, 17].

In order to perform the planned wear tests with abrasive material which is of general availability on the market, it was decided to use abrasive material which is regularly used for grinding operations (grinding tool). For later comparison with commonly used abrasive for waterjet cutting processes, the mostly used sieve classification MESH 80 (#80) was used for the laboratory tests.

The second parameter characterizing the abrasive grain is the shape factor. This factor compares an object with a surface equivalent circle:

$$f = \frac{p_o}{p_c} \tag{1}$$

where p_o is the perimeter of the object and p_c is the perimeter of the surface equivalent circle.

These three types of corundum-based abrasives were used.

2.1.1 TSCTSK #80

TSCTSK is monocrystalline, treated corundum with cubic grains and a light rose colour, (special fused aluminium oxide) produced by TREIBACHER SCHLEIFMITTEL GmbH, Austria (Fig. 2c).

For these (fresh) grains of corundum TSCTSK #80, the largest percentage share has a fraction of the grain size from 180 to 212 μm (Fig. 2a). Distributions of grain shapes for this abrasive are shown Fig. 2b. The largest percentage share has a fraction of grains representing a 1.22 shape factor.

2.1.2 ZZK 40 #80

ZZK 40 is a special fused aluminium oxide. It is alumina-zirconia eutectic (40%) roughly angular grain–shaped and of grey colour, produced by TREIBACHER SCHLEIFMITTEL GmbH, Austria (Fig. 3c).

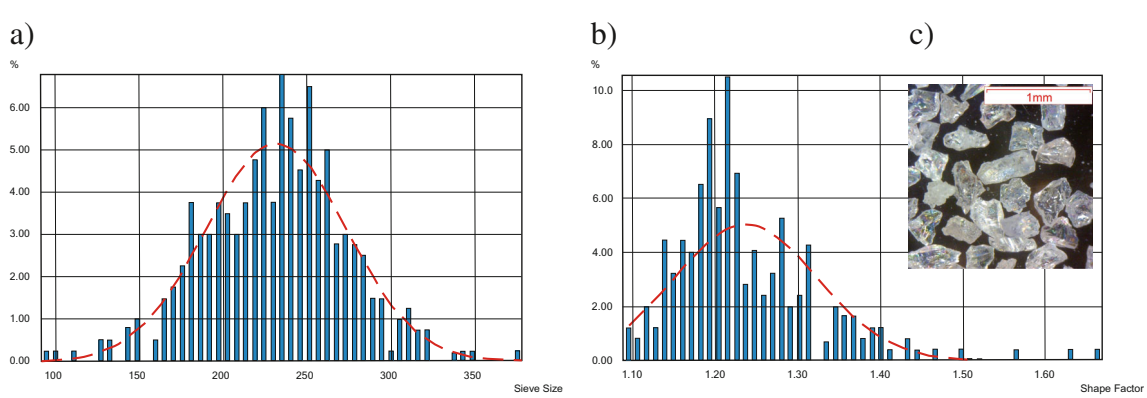

Fig. 2 Detail of corundum TSCTSK #80 abrasive: **a** particle size distribution, **b** particle shape distribution, **c** microscopic view of particle

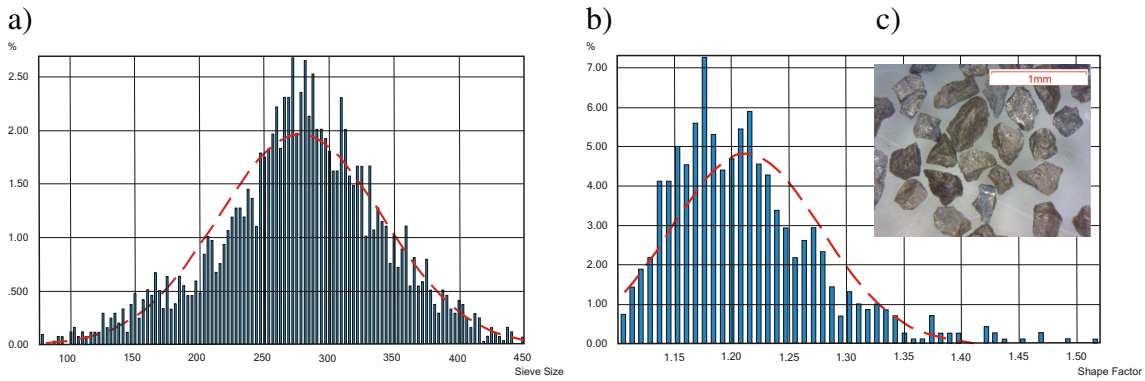

Fig. 3 Detail of corundum ZZK 40 #80 abrasive: **a** particle size distribution, **b** particle shape distribution, **c** microscopic view of particles

For these (fresh) grains of corundum ZZK 40 #80, the largest percentage share has a fraction of the grain size from 270 to 290 μm (Fig. 3a). Distributions of grain shapes for this abrasive are shown in Fig. 3b. The largest percentage share has a fraction of grains representing a 1.18 shape factor.

2.1.3 ZZWSK #120

ZWSK is white fused aluminium oxide with cubic grains (Fig. 4c), produced for specialized applications by TREIBACHER SCHLEIFMITTEL GmbH, Austria.

For these (fresh) grains of corundum ZWSK 40 #120, the largest percentage share has a fraction of the grain size from 106 to 125 μm (Fig. 4a). Distributions of grain shapes for this abrasive are shown in Fig. 4b. The largest percentage share has a fraction of grains representing a 1.14 shape factor.

2.2 Focusing tubes

For the trials focusing tubes made from unique, patented materials that are literally changing the definition of wear resistance ROCTEC®100 were used. The ROCTEC® process enables the combination of these advanced ceramic materials without the need for a soft metal binder, as is the case with tungsten carbide/cobalt using traditional sintering technology.

The ROCTEC® process enables focusing tubes to be formed using very short consolidation cycles to minimize the natural tendency of ceramic particles to grow in size when exposed to high heat for long periods. Eliminating a metallic binder and maintaining extra-fine grain size both contribute to optimum focusing tube performance. The result is an extremely durable material that very strongly resists abrasive and erosive wear [5].

3 Test procedure

Measurement of the wear on focusing tubes was examined by observing changes in

- the mass,
- the diameter of the outlet, and
- the shape of the inner bore.

In addition to the focusing tube, geometry inspection research was also conducted on

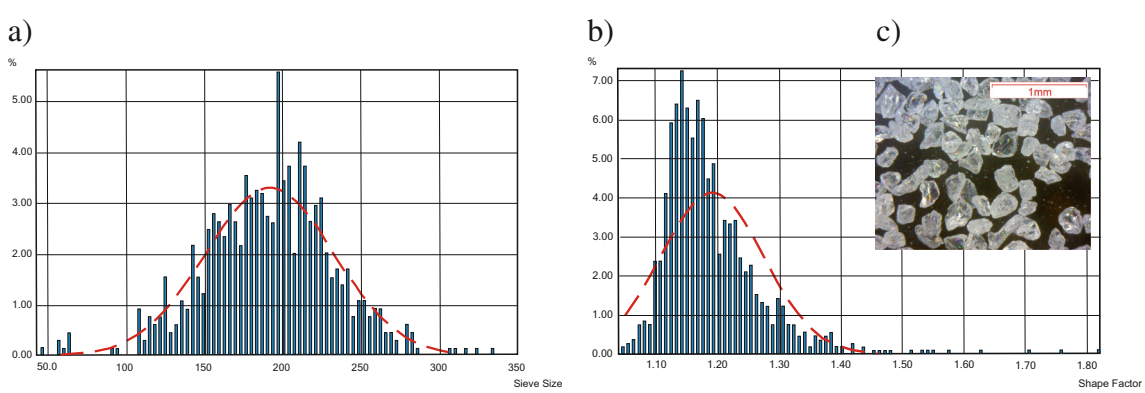

Fig. 4 Detail of corundum ZZWSK #120 abrasive: **a** particle size distribution, **b** particle shape distribution, **c** microscopic view of particles

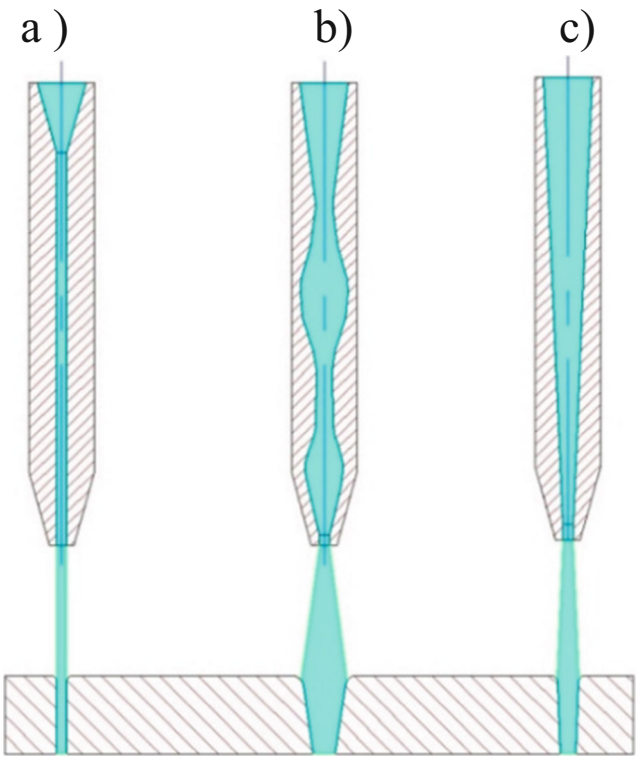

Fig. 5 Possibilities of jet shapes at the same outlet ID of the focusing tube, but different interior wear: **a** no wear, **b** uneven wear, **c** even wear

- the width of the kerf.

The status of the inner geometry of the focusing tube can be deduced from the width of the kerf. The jet shapes formed in the focusing tubes may in fact have different geometries with the same diameter of the outlet (Fig. 5).

Observation of the inner focusing tube wear was performed by casting a special plastic compound—Panasil®. It is a low viscosity, addition-curing precision impression material with very high initial hydrophilicity. Product advantages are initial hydrophilicity which lasts throughout the total working time and good flowability with high thixotropy (the property of becoming less viscous when subjected to an applied stress) [19].

The inner shape of the focusing tubes was either monitored by an indirect microscopic measurement of the cast plastic compound or a direct macroscopic measurement of the inner wall shape after an EDM cross-axial cut-off. The mass of the focusing tubes was measured by a digital scale.

A special receiver was used to capture abrasives after their exit from the focusing tube. The receiver was designed to collect the abrasives and to prevent any further particle disintegration after leaving the focusing tube. The bottom of the used PVC receiver was covered by a steel plate to prevent perforation by abrasive particles with remaining high impact forces due to high speed.

For measuring the particle size distribution of the abrasive particles, Retsch sieving equipment was used. The mass of the abrasives particles remaining on the sieves was weighed on the digital lab scale.

4 Apparatus

The study was conducted on a test rig. As a source of high pressure an intensifier BYPUMP 50APC from the Swiss company Bystronic was used. The maximum working pressure is 400 MPa at water flow of 5 dm^3/min. As a cutting tool a Bystronic cutting head was used, equipped with a water nozzle with a diameter of 0.28 mm and a focusing tube with a diameter of 0.76 mm and a length of 75 mm, mounted on a 3-axis CNC-Machine with Siemens control Sinumerik 840D. The working area of the cutting table has a dimension of 1000 × 1000 × 400 mm. The machine is equipped with an abrasive feeder and a dosing system from the Swiss company Allfi.

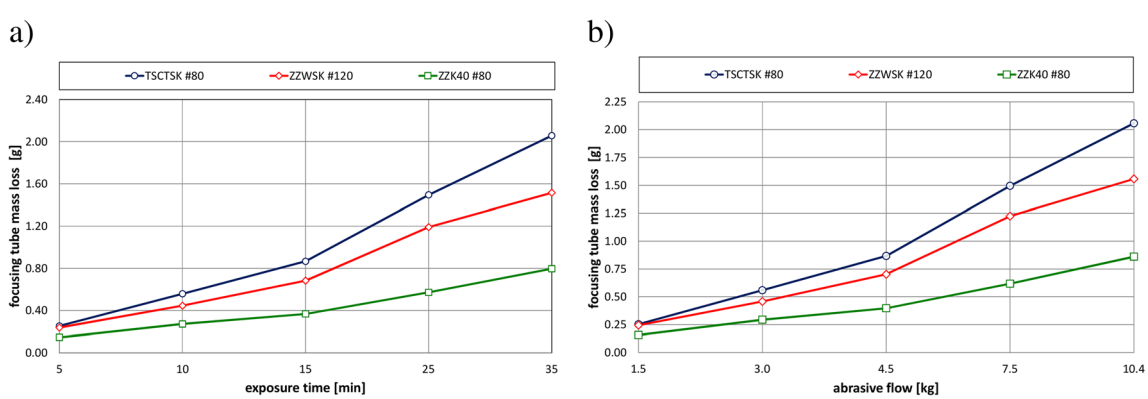

Fig. 6 Relation of focusing tube's mass loss for tested abrasive materials and **a** exposure time, **b** abrasive flow exposed to the focusing tube

Table 2 Comparison of chosen properties for corundum-based and traditional abrasives material

Abrasives	ZZWSK #120	ZZK40 #80	TSCTSK #80	GMA Garnet
Wear time factor (mg/min)	27.2	44.6	55.8	3.47 [24]

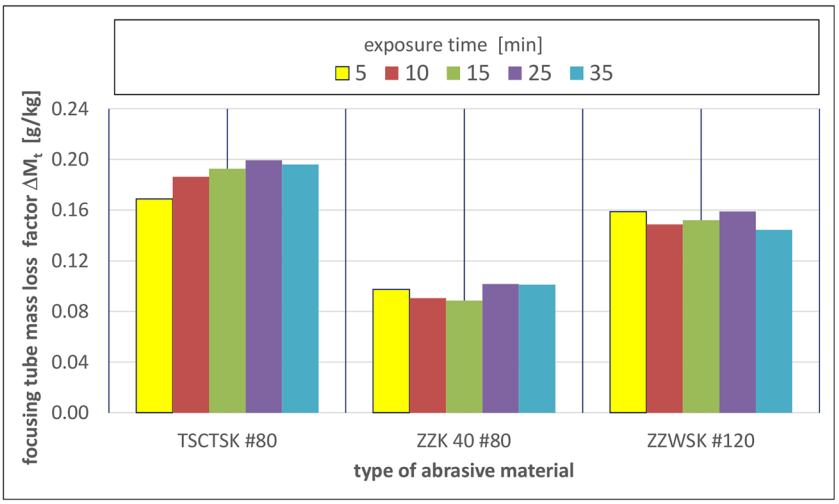

Fig. 7 Mass loss factor of focusing tubes for tested abrasive materials

5 Tests results

5.1 Focusing tube wear

5.1.1 Focusing tube's mass loss

Figure 6 presents the relation between the focusing tube's mass loss and the related working time for the tested abrasive materials. The largest focusing tube mass loss was observed for the abrasive type TSCTSK #80. After the maximum test time of 35 min, the mass loss amounted to over 2 g.

The ZZWSK corundum type caused the second largest amount of wear. After 35 min of exposure time, the loss of mass amounted to over 1.5 g. The smallest amount of mass loss in a focusing tube was observed for the abrasive type ZZK40 #80. After 35 min of exposure time, the wear and the related mass loss was almost 3 times smaller compared with TSCTSK #80 and was only 0.8 g. Also in the case of focusing tube wear, depending on the abrasive flow (Fig. 8b), the largest mass loss of a focusing tube was observed for the abrasive type TSCTSK #80.

After a maximum abrasive flow of 9.8 kg, the mass loss of the focusing tube amounted to 2 g.

The second highest amount of wear intensity is shown by corundum type ZZWSK #120. After 9.8 kg of abrasive flow, transmitted through the focusing tube, the mass loss amounted to 1.4 g. The smallest amount of mass loss in a focusing tube was observed for the abrasive type ZZK40 #80. After an abrasive flow of

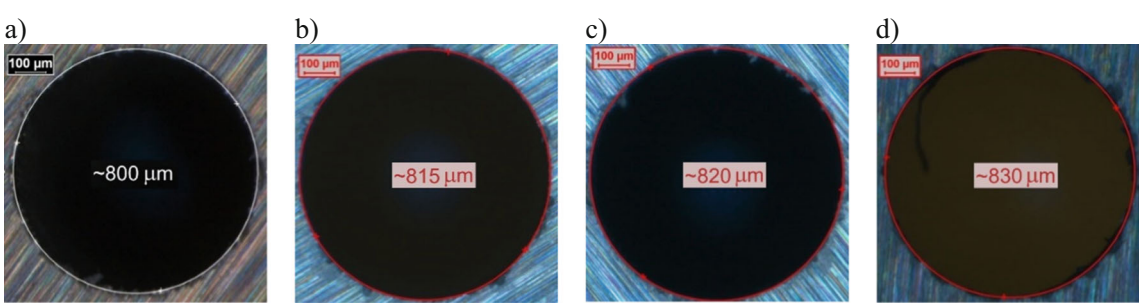

Fig. 8 Sample of focusing tube outlet IDs tested with ZZK40 #80 abrasive: **a** before cutting, **b** after 5 min, **c** after 10 min, **d** after 15 min of exposure time

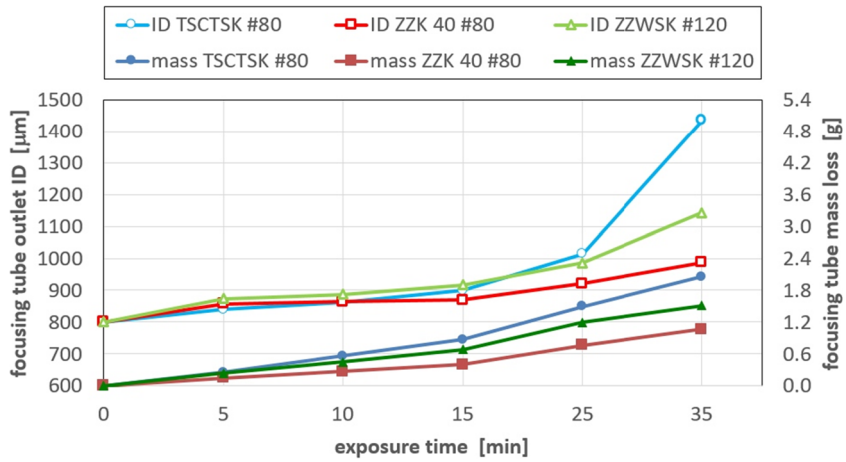

Fig. 9 Mass loss and outlet diameter of focusing tubes

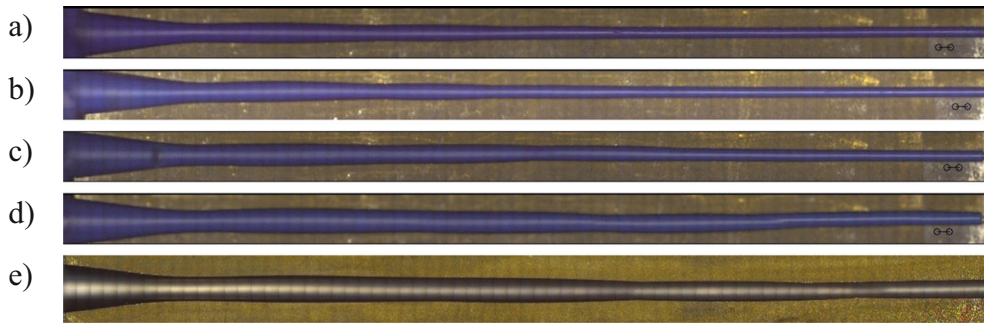

Fig. 10 View of the focusing tube inner geometry: **a** after 5 min, **b** after 10 min, **c** after 15 min, **d** after 25 min, **e** after 35 min. Parameters of machining: pressure 300 MPa, abrasive flow rate 280 g/min, abrasive TSCTSK #80

10 kg, the wear and related mass loss of the focusing tube was only 0.75 g.

Erosive properties have an effect not only on the parameters used for the cutting of materials but also on the durability of the focusing tube [1].

On the basis of this study, the possibility of calculating the focusing tube wear and related mass loss by a forecast equation was identified.

5.1.2 Time factor

The time factor $\dot{m}_t$ represents the mass loss of the focusing tube in relation to the exposure time with abrasive flow through the tube. It is calculated from the following equation:

$$\dot{m}_t = \frac{m_t}{t_w} \tag{2}$$

where m_t is the mass loss of the focusing tube (g) and t_w is the exposure time (min).

The time factor of exposure time calculated on basis Eq. (2) for the corundum-based abrasives tested is shown in Table 2.

For comparison, there is also shown the time factor for other abrasives commonly used in AWJ machining, that is GMA garnet #80. The biggest wear time factor (more than 16 times bigger than GMA garnet) has TSCTSK #80. The second in order is abrasive ZZK40 #80 with the wear time

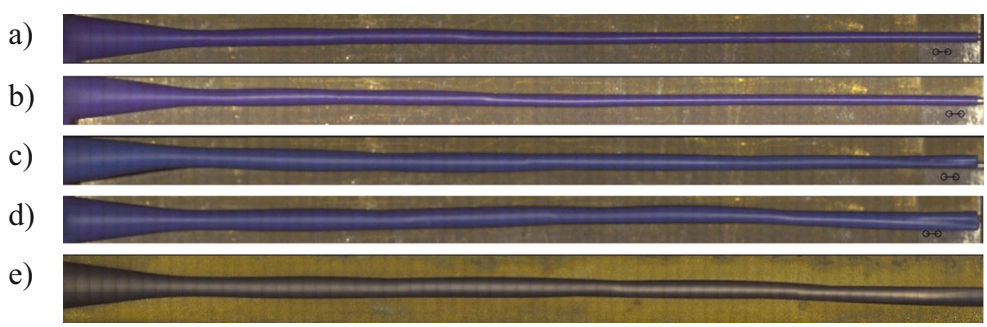

Fig. 11 View of focusing tube interior geometry: **a** after 5 min, **b** after 10 min, **c** after 15 min, **d** after 25 min, **e** after 35 min. Parameters of machining: pressure 300 MPa, abrasive flow rate 280 g/min, abrasive ZZK40 #80

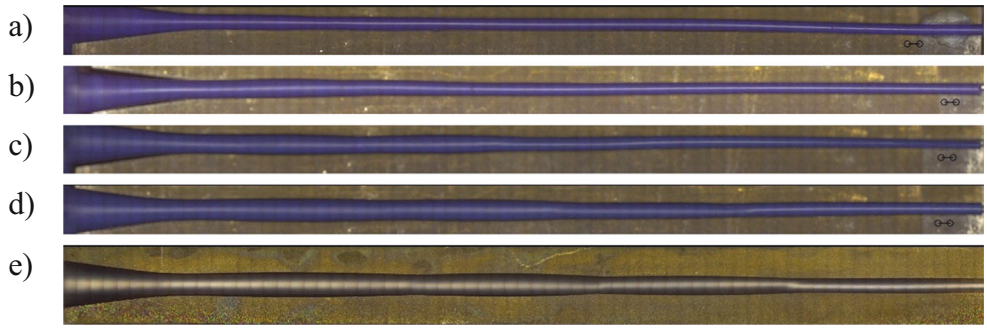

Fig. 12 View of focusing tube interior geometry: **a** after 5 min, **b** after 10 min, **c** after 15 min, **d** after 25 min, **e** after 35 min. Parameters of machining: pressure 300 MPa, abrasive flow rate 280 g/min, abrasive ZZWSK #120

factor almost 13 times bigger. Abrasive ZZWSK #120, is characterized by the smallest wear time factor but still more than almost 8 times bigger than GMA garnet #80 abrasive.

5.1.3 Mass loss factor

The mass loss factor ΔM_t is calculated by the equation

$$\Delta M_t = \frac{\dot{m}_t}{\dot{m}_a}\left[\frac{\frac{g}{min}}{\frac{kg}{min}} = \frac{g}{kg}\right] \tag{3}$$

where M_t is initial mass of the focusing tube, ΔM_t is the mass loss factor, $\dot{m}_t$ is the time-related mass loss of the focusing tube (time factor) (g/min), and $\dot{m}_a$ is the flow rate of the abrasive material (kg/min).

Figure 7 shows results of the calculations made by Eq. (3).

5.2 Monitoring of the outlet diameter of the focusing tubes

After each stage of tests, in addition to the focusing tube mass loss, the internal diameter of the outlet was also measured. Sample images are shown in Fig. 8.

The dependency of the focusing tube's ID at the outlet on the exposure time with abrasive flow inside the focusing tube is shown in Fig. 9. The exposure time of the focusing tubes for the abrasive material type TSCTSK #80 is nearly 27 min with only 0.25 mm change of the outlet diameter. For abrasive ZZWSK #120, the working time is around 33 min at 0.3 mm change of the outlet diameter.

5.2.1 The shape of the focusing tube inner geometry

The focusing tubes' internal surface wear caused by the abrasive flow is shown in Figs. 10, 11, and 12.

Qualitative changes in all cases are similar. After 5 min, wear was only observed in the transition zone of the internal cone into the cylinder. After 10 min of work, the wear in this zone increased and wear signs appeared in the middle part of the focusing tube. After 15 min, wear in these zones continued to grow. After 25 min, a further increase was observed. In the outlet area, appearance of wear was observed. It was particularly intense for ZZK40 #80 abrasives. After being in operation for 35 min, in all cases, a further increase in wear was observed in all zones. In the outlet zone, the smallest wear was caused by abrasive ZZWSK #120, and the largest wear was caused by abrasive ZZK40 #80.

Such uneven wear is caused by the process of generating an abrasive waterjet. A stream of clean water at high speed (even 800 m/s) enters the focusing tube at the bottom of the mixing chamber (see Fig. 1b) and reduces the usable open diameter of the conical inlet for the abrasive grains. Before abrasive grains enter the jet, they are reflected many times from the external jet surface and the inner surface of the focusing tube and cause its varied wear.

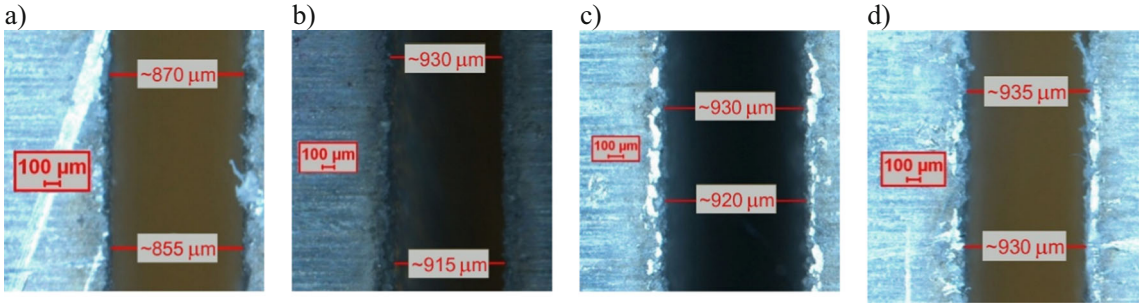

Fig. 13 Samples of kerfs cut with ZZK40 #80 abrasive: **a** start of cut, **b** after 5 min, **c** after 10 min, **d** after 15 min

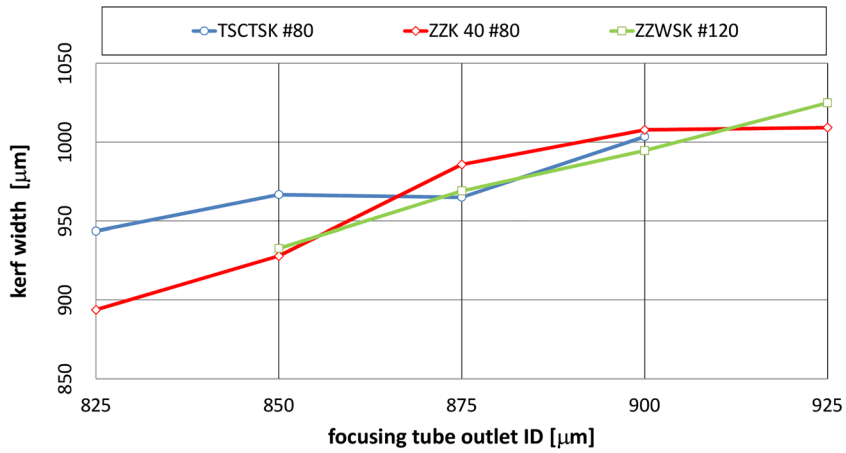

Fig. 14 Relation between focusing tube outlet ID and width of cutting kerf

5.2.2 Width of the cutting kerf

The sample view of the cutting kerfs in the work pieces depends on the focusing tube's wear shown in Fig. 13. An increase in the width of the cutting kerf as a function of the focusing tube's wear, specifically in the function of increasing the outlet diameter in the focusing tube just after the start and after cutting for 5, 10, and 15 min can be observed.

The dependence of the cutting kerf's width on the focusing tube outlet diameter is shown in Fig. 14. For all three tested abrasives, a direct proportional dependency can be observed. For abrasives ZZK40 #80 and ZZWSK #120, almost identical trend lines can be seen.

5.3 Disintegration of abrasive grains

5.3.1 TSCTSK #80

For corundum type TSCTSK #80 with an initial grain shape and size, the largest percentage of the grain size distribution can be found at 275 μm diameter (Fig. 15a). After passing through the mixing chamber and the focusing tube, the grain size distribution remains almost identical (see Fig. 15b). Also after the cutting process, the grain size distribution remains stable because of the minimal disintegration of the very hard grains (compared with the target material hardness) (Fig. 15c).

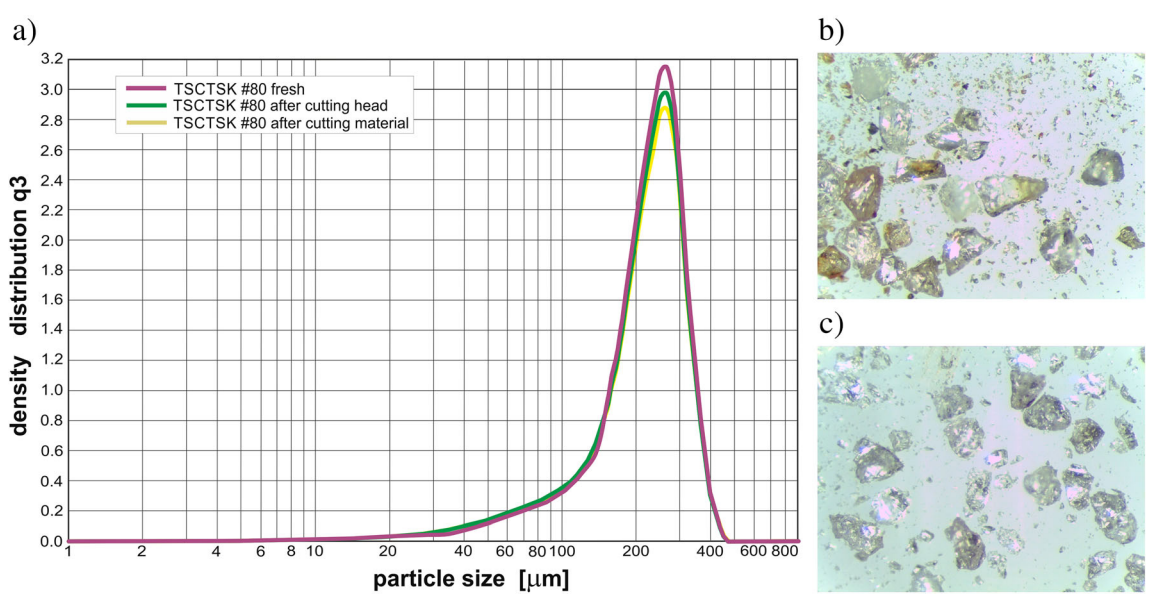

Fig. 15 TSCTSK #80 grains: **a** particle size distribution, **b** view of disintegrated grains after the mixing process in the cutting head, **c** view of disintegrated grains after cutting of the target material

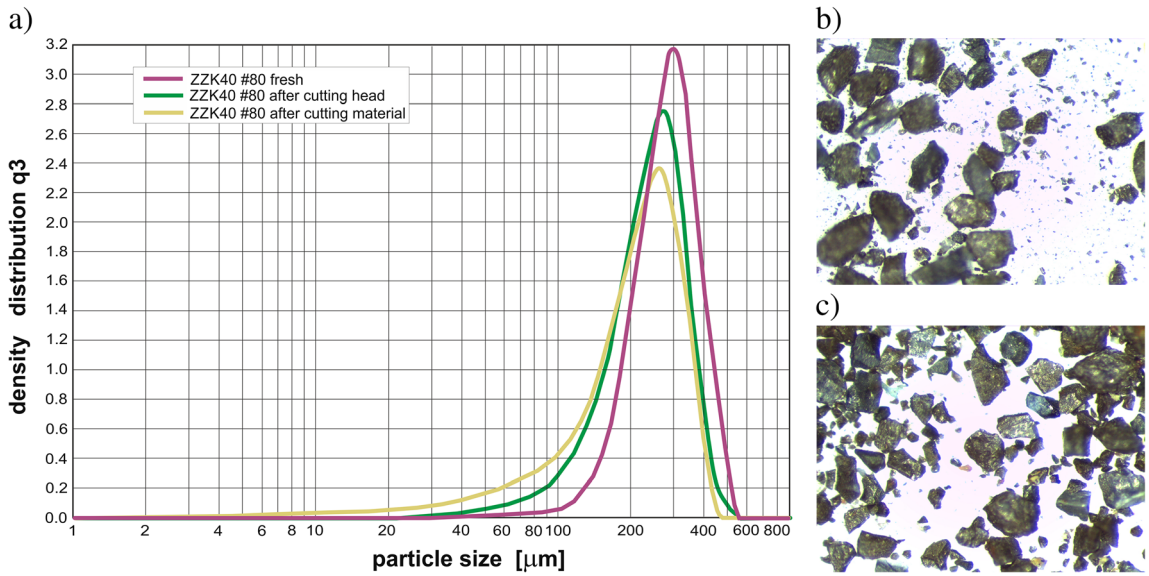

Fig. 16 ZZK40 #80 grains: **a** particle size distribution, **b** view of disintegrated grains after the mixing process in the cutting head, **c** view of disintegrated grains after cutting of the target material

5.3.2 ZZK40 #80

For the corundum type ZZK40 #80 with an initial grain shape and size, the largest percentage of the grain size distribution can be found at 300 µm diameter (Fig. 16a). After the cutting process, a decrease in the max. particle diameter can be observed. After passing through the mixing chamber and the focusing tube, the grain size distribution shows a shift to smaller particles (highest percentage at 285 µm) (see Fig. 16b). The grain size distribution shows an additional shift towards the highest percentage of the particle diameter at 270 µm (Fig. 16c).

5.3.3 ZZWSK #120

For corundum type ZZWSK #120 with an initial grain shape and size, the largest percentage of the grain size distribution can be found at 220 µm diameter (Fig. 17a). After passing through the mixing chamber and the focusing tube, the grain size distribution shows a shift to smaller particles (highest percentage at 210 µm) (see Fig. 17b). After the cutting process, a decrease in the max. particle diameter can be observed. The grain size distribution shows an additional shift towards the highest percentage of the particle diameter at 200 µm (Fig. 17c).

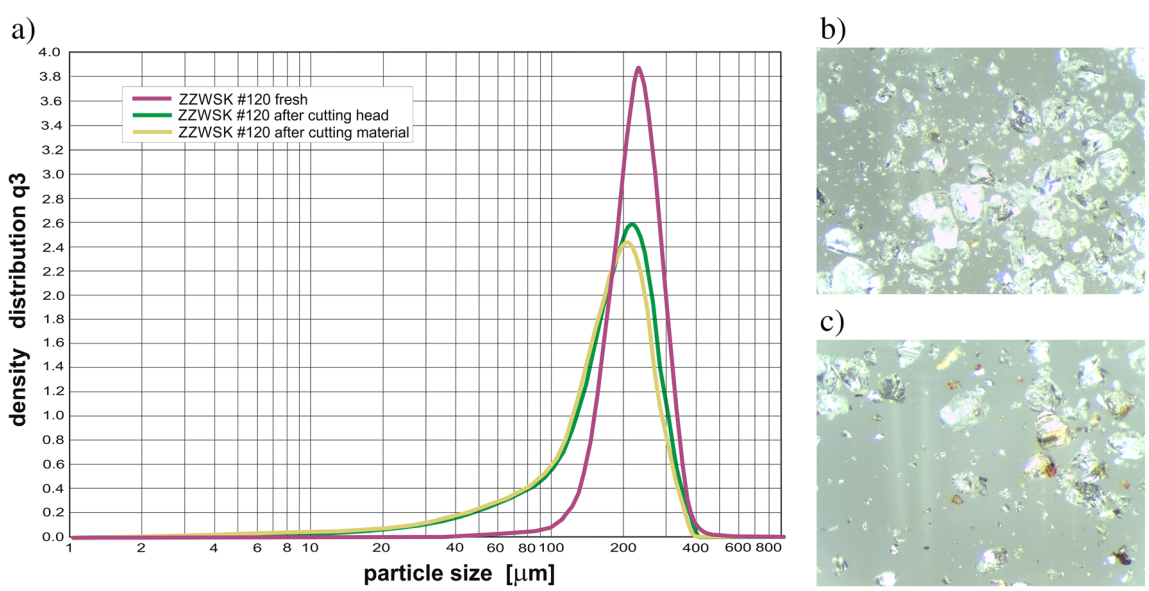

Fig. 17 ZZWSK #120 grains: **a** particle size distribution, **b** view of disintegrated grains after the mixing process in the cutting head, **c** view of disintegrated grains after cutting of the target material

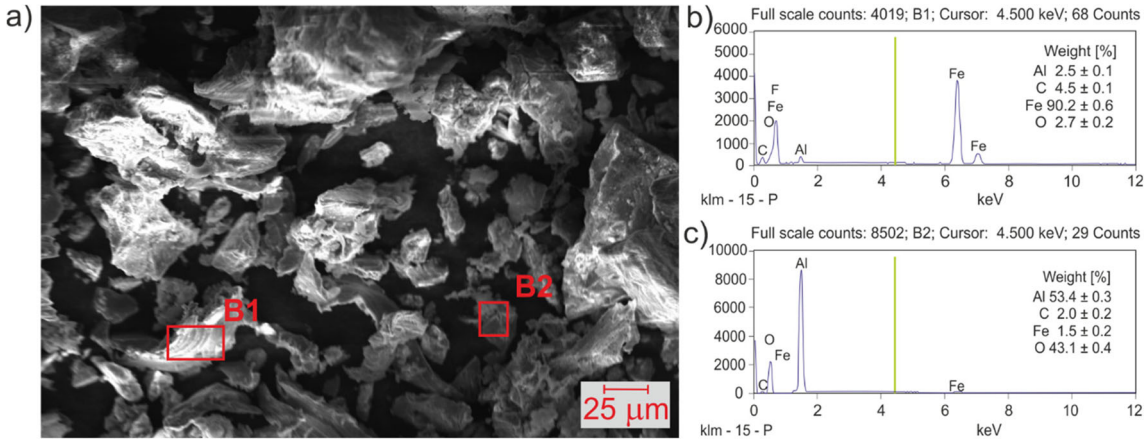

Fig. 18 Sample of microscopic view (**a**) and chemical composition of caught particles after cutting steel with TSCTSK #80 abrasive; B1, steel chip (**b**); B2, corundum grain (**c**)

5.4 Particle identification after cutting process

The used abrasive grains together with the in-process generated microchips were caught by a special PVC catcher tank. After a drying process, the abrasive grains were separated from the chips and were observed and analysed by an SEM microscope. Figure 18a shows SEM micrographs of the steel chips (example area 1) and TSCTSK abrasive grains (example area 2). Further research has been made for the identification of material chips and abrasive grains through the investigation of chemical compositions at the locations observed using EDX spectroscopy analysis. In Fig. 18b, iron and carbon are the major compositions. This confirms that these are steel chips. In area 2, the dominant elements are aluminium and oxygen (Fig. 18c), which confirms that there is the corundum grain.

Figure 19a shows SEM micrographs of the corundum ZZK40 grains (steel chips area 1) and steel chips (area 2). It is confirmed by EDX spectroscopy analysis. In Fig. 19b, aluminium and oxygen are the main compositions which confirm that there is the corundum grain. In area 2, the dominant elements are iron and carbon (Fig. 19c). It suggests that there are steel chips.

The ZZWSK corundum abrasives (area 2) and steel chips (area 3) are presented in next SEM micrographs (Fig. 20a). Also, in this case, it is confirmed by EDX spectroscopy analysis. In area 2 in Fig. 20b, the primary compositions are aluminium and oxygen, which confirms that there is the corundum grain. In area 3, the dominant elements are iron and carbon (Fig. 20c), which confirms that there are steel chips.

A small amount of iron was observed on all abrasive grains that were transferred during the cutting process. Small amounts of aluminium and oxygen were also observed on steel chips. This suggests a small transfer of disintegrated abrasive to the surface of erosion products (chips).

The results of the SEM analysis show the possibility of organizing final quality control of the separation process. Difference in colour can be used for a first (cost-saving) quick test.

If necessary, a 100% process monitoring of the separation process can be qualified. Especially for medical applications

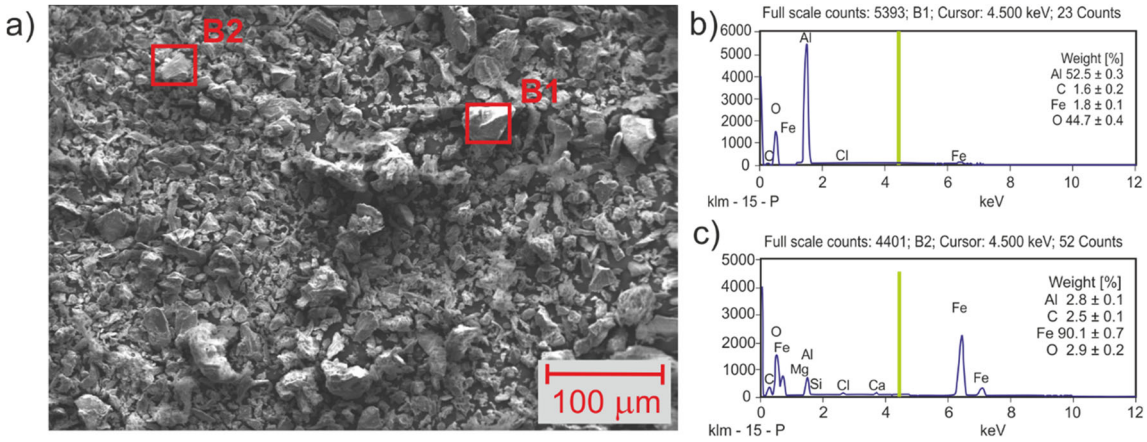

Fig. 19 Sample of microscopic view (**a**) and chemical composition of caught particles after cutting steel with ZZK40 #80 abrasive; B1, corundum grain (**b**), B2, steel chip (**c**)

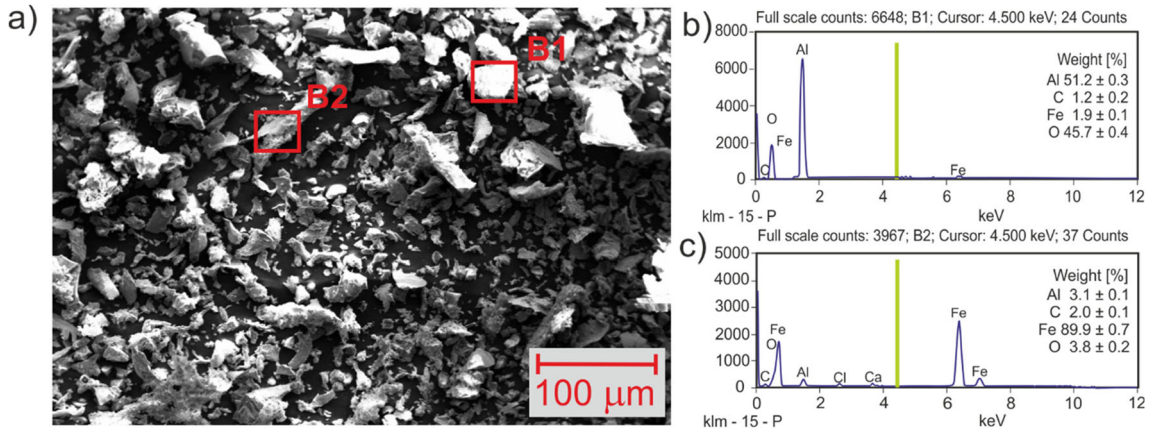

Fig. 20 Sample of microscopic view (**a**) and chemical composition of caught particles after cutting steel with ZZWSK #120 abrasive; B1, corundum grain (**b**); B2, steel chip (**c**)

of the re-used grains, a chip-free recycled abrasive grain material must be guaranteed.

6 Conclusions

Based on the research, following conclusions can be drawn:

- High hardness values of corundum-based abrasive (9 Mohs) in relation to common garnet (7.5 Mohs) cause negative increase of wear inside the focusing tube.
- Detailed wear tests by corundum-based abrasives show that focusing tube wear is 8 to 16 times bigger than in case commonly used abrasive, garnet.
- Process-related particle and material interaction (corundum grains vs. hard metal tube wall and corundum grains vs. target material (e.g. steel)) show very stable shape and size of grains (due to higher hardness).
- The observed shape and size stability of the abrasive grains can serve as the basis for an efficient recycling process.
- The good cutting and recycling properties of the tested corundum-based abrasive mean that it can be used for cutting of very hard materials.
- The mass loss factor of the used focusing tubes observed in tests shows different trends for different corundum materials.
- Observed modification shape of the inner tube geometry is caused by an increase in wear in the direction of flow through the tube in the starting phase of the cutting process.
- After 15 min of focusing tubes exposed to each corundum-based abrasive, a big increasing of the wear (both mass loss and outlet ID) was observed, most for TSCTSK abrasives.
- Long-time use of focusing tubes exposed to wear by corundum particle contact will lead to a loss of cutting precision.
- The application of corundum-based abrasives can only be recommended under certain economic conditions.

References

1. Barlić J, Nedić B, Marušić V (2008) Focusing tube wear and quality of the machined surface of the abrasive water jet machining. Tribol Ind 30:55–58
2. Carach J, Lehocka D, Legutko S, Hloch S, Chattopadhyaya S, Dixit AR (2018) Surface roughness of graphite and aluminium alloy after hydro-abrasive machining. In: Hamrol A, Ciszak O, Legutko S, Jurczyk M (eds) Advances in manufacturing (manufacturing 2017). Springer International Publishing Ag, Cham, pp 805–813
3. Chen X, Guan J, Deng S, Liu Q, Chen M (2018) Features and mechanism of abrasive water jet cutting of Q345 steel. Int J Heat Technol 36:81–87. https://doi.org/10.18280/ijht.360111
4. Corundum. The mineral corundum, sapphire, ruby info & pictures. https://www.minerals.net/mineral/corundum.aspx. Accessed 21 Jul 2018
5. Galecki G, Mazurkiewicz M (1987) Hydro-abrasive cutting head—energy transfer efficiency. In: Proceeding of the Fourth U.S. Water Jet Conference. pp 172–177
6. Hreha P, Radvanska A, Knapcikova L, Krolczyk GM, Legutko S, Krolczyk JB, Hloch S, Monka P (2015) Roughness parameters calculation by means of on-line vibration monitoring emerging from Awj interaction with material. Metrol Meas Syst 22:315–326. https://doi.org/10.1515/mms-2015-0024
7. Kacalak W, Lipiński D, Bałasz B, Rypina Ł, Tandecka K, Szafraniec F (2018) Performance evaluation of the grinding wheel with aggregates of grains in grinding of Ti-6Al-4V titanium alloy. Int J Adv Manuf Technol 94:301–314. https://doi.org/10.1007/s00170-017-0905-x
8. Kukielka L (2010) New damping models of metallic materials and its application in non-linear dynamical cold processes of metal forming. Steel Res Int 81:1482–1485
9. Kukiełka K (2016) Ecological aspects of the implementation of new technologies processing for machinery parts. Rocznik Ochrona Srodowiska Annu Set Environ Prot 18:137–157
10. Kukielka K, Kukielka L (2006) Modeling and numerical analysis of the thread rolling process. Pamm 6:133–134. https://doi.org/10.1002/pamm.200610
11. Kündig R, Bühler C, Surbeck H Aluminium oxide (corundum, emery, sapphire/ruby). ETHZ, Zurich

12. Leonarcik R, Urbaniak M, Debkowski R (2018) Method for assessing the grinding wheels operational properties. Eksploat Niezawodn 20:531–541. https://doi.org/10.17531/ein.2018.4.4
13. Lipinski D, Kacalak W (2016) Metrological aspects of abrasive tool active surface topography evaluation. Metrol Meas Syst 23:567–577. https://doi.org/10.1515/mms-2016-0043
14. Martin GR, Lauand CT, Hennies WT, Ciccu R (2000) Abrasives in water jet cutting systems. Balkema Publishers, Leiden
15. Martinec P, Foldyna J, Sitek L, Ščučka J, Vašek J (2002) Abrasives for AWJ cutting. INCO-COPERNICUS No. Institute of Geonics, Ostrava, 2002, ISBN 80-86407-02-0
16. Nadolny K (2014) State of the art in production, properties and applications of the microcrystalline sintered corundum abrasive grains. Int J Adv Manuf Technol 74:1445–1457. https://doi.org/10.1007/s00170-014-6090-2
17. Nadolny K, Sutowski P, Herman D (2015) Analysis of aluminum oxynitride AlON (Abral®) abrasive grains during the brittle fracture process using stress-wave emission techniques. Int J Adv Manuf Technol 81:1961–1976. https://doi.org/10.1007/s00170-015-7338-1
18. Nag A, Scucka J, Hlavacek P, Klichova D, Srivastava AK, Hloch S, Dixit AR, Foldyna J, Zelenak M (2018) Hybrid aluminium matrix composite AWJ turning using olivine and Barton garnet. Int J Adv Manuf Technol 94:2293–2300. https://doi.org/10.1007/s00170-017-1036-0
19. Panasil initial contact Light (1:1) - Kettenbach GmbH & Co. KG. http://www.kettenbach.de/en/dental/products/precision-impression/a-silicones/panasil-initial-contact-light-11.html. Accessed 21 Jul 2018
20. Patyk R, Kukielka L, Kaldunski P, Bohdal L, Chodor J, Kulakowska A, Kukielka K, Nagnajewicz S (2018) Experimental and numerical researches of duplex burnishing process in aspect of achieved productive quality of the product. AIP Conf Proc 1960: 070021. https://doi.org/10.1063/1.5034917
21. Perec A (2012) Comparison of abrasive grain disintegration during the formation abrasive water jet and abrasive slurry injection jet. In: BHR Group - 21st International Conference on Water Jetting: Looking to the Future, Learning from the Past. pp 319–327
22. Perec A (2016) Abrasive suspension water jet cutting optimization using orthogonal array design. Procedia Eng 149:366–373. https://doi.org/10.1016/j.proeng.2016.06.680
23. Perec A (2018) Experimental research into alternative abrasive material for the abrasive water jet cutting of titanium. Int J Adv Manuf Technol 97:1529–1540. https://doi.org/10.1007/s00170-018-1957-2
24. Perec A (2018) Environmental aspects of abrasive water jet cutting. Annu Set Environ Prot Rocznik Ochrona Srodowiska 20:258–274
25. Perec A, Pude F, Stirnimann J, Wegener K (2015) Feasibility study on the use of fractal analysis for evaluating the surface quality generated by waterjet. Tehnički vjesnik 22:879–883. https://doi.org/10.17559/TV-20140128231244
26. Perec A, Pude F, Kaufeld M, Wegener K (2017) Obtaining the selected surface roughness by means of mathematical model based parameter optimization in abrasive waterjet cutting. Strojniški vestnik J Mech Eng 63:606–613. https://doi.org/10.5545/sv-jme.2017.4463
27. Spadło S, Krajcarz D (2018) Study of the geometrical structure of copper surface after abrasive waterjet cutting. IOP Conf Ser Mater Sci Eng 461:012045. https://doi.org/10.1088/1757-899X/461/1/012045
28. Sutowski P, Sutowska M, Kaplonek W (2018) The use of high-frequency acoustic emission analysis for in-process assessment of the surface quality of aluminium alloy 5251 in abrasive waterjet machining. Proc Inst Mech Eng B J Eng Manuf 232:2547–2565. https://doi.org/10.1177/0954405417703428
29. Tavodová M (2013) The surface quality of materials after cutting by abrasive water jet evaluated by selected methods. Manuf Technol 13:236–241
30. The free dictionary Corundum, artificial. In: Encyclopedia2. http://encyclopedia2.thefreedictionary.com/. Accessed 1 Jul 2018
31. Valicek J, Drzik M, Hloch S, Ohlidal M, Miloslav L, Gombar M, Radvanska A, Hlavacek P, Palenikova K (2007) Experimental analysis of irregularities of metallic surfaces generated by abrasive waterjet. Int J Mach Tools Manuf 47:1786–1790. https://doi.org/10.1016/j.ijmachtools.2007.01.004
32. Wessels V, Grigoryev A, Dold C, Wyen C-F, Roth R, Weingaertner E, Pude F, Wegener K, Loeffler JF (2012) Abrasive waterjet machining of three-dimensional structures from bulk metallic glasses and comparison with other techniques. J Mater Res 27:1187–1192. https://doi.org/10.1557/jmr.2012.36
33. Wojcik R, Nadolny K (2017) Effects of a variety of cutting fluids administered using the minimum quantity lubrication method on the surface grinding process for nickel-based alloys. J Zhejiang Univ-SCI A 18:728–740. https://doi.org/10.1631/jzus.A1600416

Publisher's note Springer Nature remains neutral with regard to jurisdictional claims in published maps and institutional affiliations.